Optics Letters

# Compact and cost-effective temperature-insensitive bio-sensor based on long-period fiber gratings for accurate detection of *E. coli* bacteria in water

Krishnendu Dandapat,[1] Saurabh Mani Tripathi,[1,*] Yasser Chinifooroshan,[2] Wojtek J. Bock,[2] and Predrag Mikulic[2]

[1]Department of Physics, Indian Institute of Technology Kanpur, Uttar Pradesh 208016, India
[2]Photonics Research Centre, Department of Computer Science and Engineering, University of Quebec in Outaouais, Gatineau, Quebec J8Y 3G5, Canada
*Corresponding author: smt@iitk.ac.in

Received 14 June 2016; revised 5 August 2016; accepted 13 August 2016; posted 22 August 2016 (Doc. ID 268231); published 8 September 2016

**We propose and demonstrate a novel temperature-insensitive bio-sensor for accurate and quantitative detection of *Escherichia coli* (*E. coli*) bacteria in water. Surface sensitivity is maximized by operating the long-period fiber grating (LPFG) closest to its turnaround wavelength, and the temperature insensitivity is achieved by selectively exciting a pair of cladding modes with opposite dispersion characteristics. Our sensor shows a nominal temperature sensitivity of ~1.25 pm/°C, which can be further reduced by properly adjusting the LPFG lengths, while maintaining a high refractive index sensitivity of 1929 nm/RIU. The overall length of the sensor is ~3.6 cm, making it ideally suitable for bio-sensing applications. As an example, we also show the sensor's capability for reliable, quantitative detection of *E. coli* bacteria in water over a temperature fluctuation of room temperature to 40°C.** 

***OCIS codes:*** (050.2770) Gratings; (060.2370) Fiber optics sensors; (120.0280) Remote sensing and sensors; (060.3735) Fiber Bragg gratings.

http://dx.doi.org/10.1364/OL.41.004198

Temperature cross-sensitivity is one of the primary causes of errors associated with the practical applications of fiber-optic bio-sensors. Since the refractive index of bio-chemical samples and the waveguide regions changes with temperature, often a precise determination of the refractive index (RI) needs temperature isolation/calibration [1–3]. Many innovative methods have recently been proposed to resolve the temperature cross-sensitivity, including making use of both resonances of dual-resonance long-period fiber gratings (DRLPFGs) [4], concatenating fiber Bragg gratings with long-period gratings [5], concatenating LPFGs in double cladding fibers [6], employing core and cladding materials with different thermo-optic coefficients [7], and coating suitable polymer materials on the fiber surface [8]. Although very innovative in compensating the temperature cross-sensitivity, these methods also suffer from certain drawbacks associated with the customized fiber design, increased sensor and detection unit cost, and reduced RI sensitivity due to overlay coating.

To overcome these issues, we recently demonstrated a temperature-insensitive RI sensor based on concatenated DRLPFGs with an appropriate inter-grating space (IGS) between them [9]. Each grating was tuned to the DRLPFG regime by partially etching the cladding over the grating region, making the phase difference ($\Delta\beta = \beta_c - \beta_{cl}$) between the two modes involved of opposite spectral nature to that of the unetched IGS region for $\lambda > \lambda_D$. ($\lambda_D$ is the turnaround wavelength for the DRLPFG.) As a result, the resonance wavelengths over the higher wavelength side of the turnaround wavelength ($\lambda > \lambda_D$) became temperature insensitive for an appropriate length of IGS [9]. The required IGS length, however, was quite long (~20 cm) due to the same thermo-optic coefficients of the grating and IGS regions, increasing the overall sensor length. For bio-sensing applications, on the other hand, typically a smaller sensor length is preferred to avoid the waste of bio-samples [10].

In this Letter, we present a novel and cost-effective method to compensate for the temperature-induced phase changes of LPFGs by selective excitation of the cladding modes of opposite dispersion characteristics by means of optimized concatenated LPFGs. The resultant sensor is extremely sensitive to changes in ambient refractive indices, with the sensitivity being 1929 nm/RIU, over the biologically relevant ambient refractive index (ARI) range of 1.333–1.353, displaying the capability of detecting an index variation of $\sim 5 \times 10^{-6}$ RIU in the ARI using a detection system with a resolution of 10 pm, with a negligible temperature sensitivity of −1.25 pm/°C over a temperature variation of 40°C.

The schematic diagram of our sensor structure is shown in Fig. 1, which consists of two concatenated LPFGs with

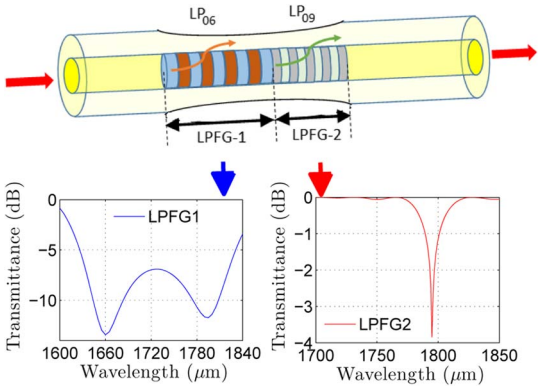


**Fig. 1.** Schematic diagram of the sensor structure.

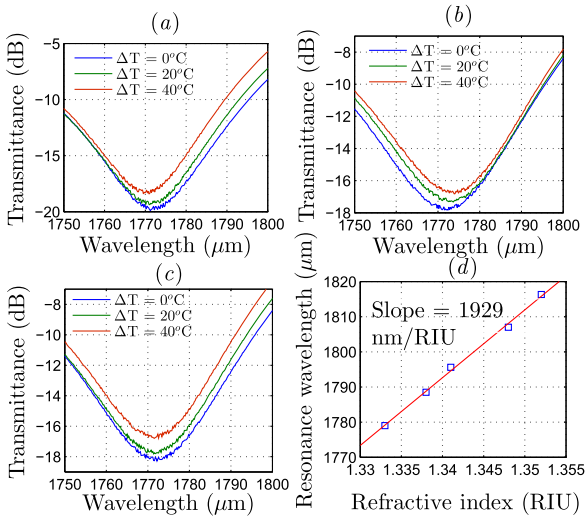


**Fig. 2.** Transmission spectrum for sensors employing a LPFG2 length of (a) 2.6 cm, (b) 2.8 cm, and (c) 2.64 cm. (d) Variation of $\lambda_R$ with ARI for a LPFG2 length of 2.64 cm.

opposite dispersion characteristics. To fabricate our sensor, we first inscribed single resonance photosensitive LPFGs in a SMF-28 optical fiber (Corning, New York 14831, USA) using a chromium amplitude mask with a varying period ($\Lambda =$ 226.8 μm and 358 μm) and KrF excimer laser (Lumonics Lasers, Pulse Master-840) emitting at 248 nm at a pulse repetition rate of 100 Hz, a pulse duration of 12 ns, and a peak pulse energy of 10 mJ. The grating length of LPFG1 ($\Lambda = 226.8$ μm) was fixed at 1 cm and that of LPFG2 was varied between 2.5 and 3.0 cm. The gratings fabricated in this way have resonance wavelengths at 1245 and 1310 nm, respectively. We then annealed the gratings at 150°C for 4 h to release the excess hydrogen and stabilize their optical properties. The cladding region of both the gratings was then partially etched to tune the LPFG1 into a dual resonance regime [9] and match its higher resonance wavelength with that of the LPFG2. It is important to mention here that for the practical application of the temperature-insensitive sensor, for a given temperature fluctuation the spectral shift to resonance bandwidth ratio of the individual LPFGs should be close to each other. The ratios for the two LPFGs used in this Letter are 0.18 and 0.16. The grating periods and their respective lengths were optimized in such a way that the excited cladding modes (1) are orthogonal modes and thus, do not interfere with each other [11,12], and (2) do not couple any power back to the fundamental mode of the optical fiber once they are concatenated. This is important to insure a modal interference-free transmission spectrum which is extremely important for bio-sensing applications. To achieve temperature insensitivity, the length of the LPFG1 was fixed at 1 cm and that of the LPFG2 was varied. Further, to avoid the microbend and strain-induced errors, we maintained a constant tension along the fibers throughout the experiments by attaching the fiber near one end of the LPFG and applying a fixed force near the other end of it. The temperature response of the transmission spectrum (recorded using a Yokogawa long wavelength optical spectrum analyzer AQ6375B) for sensors employing two different lengths of LPFG2, 2.6 and 2.8 cm, subjected to temperature variations of 0°C, 20°C, and 40°C, with respect to room temperature, are plotted in Figs. 2(a) and 2(b), respectively.

In Fig. 2(a), the resonance minima near 1770 nm show a blue spectral shift with increasing temperature whereas, in Fig. 2(b), the resonance minima show redshift with respect to the same temperature variations. Evidently, at an optimum length ratio, the sensor should be temperature insensitive. This has been shown in Fig. 2(c), where we have plotted the transmission spectrum of the sensor employing a length of 2.64 cm for LPFG2. A nominal spectral shift of ~50 pm (least count of our experiment) is observed for a temperature variation of 40°C, establishing a temperature sensitivity of 1.25 pm/°C. We would like to mention here that limited by the periods of amplitude mask used in this Letter, the temperature insensitivity has been obtained in a higher wavelength regime. Nevertheless, using amplitude masks of smaller grating periods, the temperature insensitivity can be obtained at a relatively lower wavelength regime using the same principle as proposed in the current study. Next, we measured the refractive index sensitivity of the sensor by immersing the sensor in samples of different refractive indices varying between biologically relevant ambient refractive index range of 1.333–1.353 [10], prepared by dissolving various volumes of glycerin in distilled water. The response is plotted in Fig. 2(d), showing a red spectral shift of 1929 nm/RIU. The sensor is thus capable of detecting an index variation of $\sim 5 \times 10^{-6}$ RIU in the biosamples using a detector with a resolution of 10 pm. We would like to mention here that owing to the guided mode's tendency to shift toward regions of a higher refractive indices [11,12], the RI sensitivity of our sensor can be further increased by increasing the ambient RI of the sample. For our experiments, however, we limited the measurements only to the biologically relevant RI range of 1.333–1.353 [10].

To understand the origin of temperature insensitivity theoretically, we consider an optical fiber with core and cladding regions made of 3.1 mol. % $GeO_2$ doped $SiO_2$ and fuzzed $SiO_2$; their radii ($r_c$ and $r_{cl}$) are assumed as 4.1 μm and 55 μm, respectively. A smaller cladding radius, as compared to the standard 62.5 μm, is taken in our calculations to incorporate etched cladding of the experimental sensor. Unless stated otherwise, the ambient RI is taken as 1.333. We used a Sellmeier relation to obtain the wavelength dependent RIs of core and cladding regions [13]. Using these parameters, the spectral variation of a propagation constant difference ($\beta_c - \beta_{cl}$) for $LP_{01} - LP_{09}$ and $LP_{01} - LP_{06}$ modal coupling is shown in Figs. 3(a) and 3(b), respectively. The slopes of $\Delta\beta$ versus

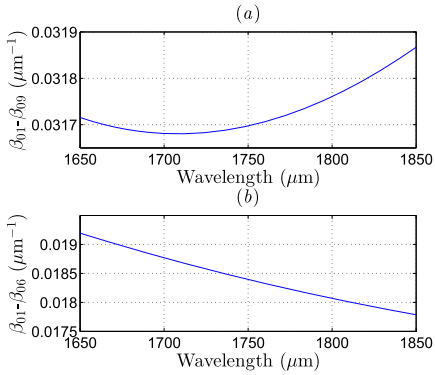


**Fig. 3.** Dispersion curves for (a) the $LP_{01}$ – $LP_{09}$ mode and (b) the $LP_{01}$ – $LP_{06}$ mode coupling in a germanio-silicate optical fiber with a core made of 3.1 mol. % $GeO_2$ doped $SiO_2$.

the wavelength curve are of an opposite nature for wavelengths larger than 1700 nm, showing the opposite dispersion characteristics of the two modal couplings for wavelengths larger than the turnaround wavelength of $LP_{01}$ – $LP_{09}$ modal coupling. Since the sensitivity of LPFG-based sensors is proportional to the slope of $\beta_c - \beta_{cl}$ versus wavelength curve, the expected sensitivities of the LPFGs based on the two modal couplings should be of the opposite nature. At an optimum length ratio of the two LPFGs, the net phase introduced by one grating can thus be canceled by that introduced by the second grating. To show this more clearly, in Fig. 4, we have plotted the theoretically obtained transmission spectrum, using the matrix method [14], for individual gratings and a combination of the two, showing a temperature-insensitive transmission spectrum for LPFG1 and LPFG2 lengths of 3 and 1.85 cm, respectively. Figures 4(a) and 4(b) show the transmission spectrum of the two LPFGs corresponding to $LP_{01}$ – $LP_{09}$ and $LP_{01}$ – $LP_{06}$ modal coupling; their respective grating periods are taken as 195.68 and 340.83 μm. As expected, with an increasing temperature, the LPFG1 shows blue spectral shift, whereas

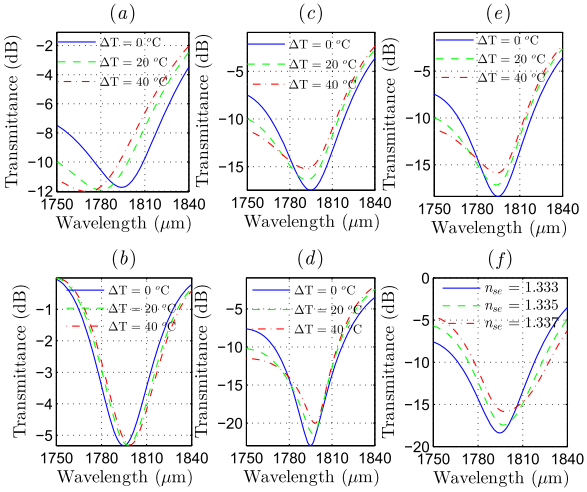


**Fig. 4.** Theoretical transmission spectrum at different temperature differences for (a) LPFG-1, (b) LPFG-2, (c) $l_{LPFG2} = 1.75$ cm, (d) $l_{LPFG2} = 2.2$ cm, and (e) $l_{LPFG2} = 1.85$ cm. (f) Effect of changing ARI on a temperature-insensitive sensor.

the LPFG2 shows red spectral shift. Next, keeping the length of LPFG1 as 3 cm, the transmission spectrum of the concatenated LPFGs corresponding to LPFG2 length of 1.75 and 2.20 cm, are plotted in Figs. 4(c) and 4(d), showing a blue spectral shift for the former and a red spectral shift for the latter. Finally, the temperature-insensitive spectrum is obtained for an LPFG2 length of 1.85 cm, and has been plotted in Fig. 4(e) at different temperatures. The sensor's response with changing ARIs is shown in Fig. 4(f) showing a spectral shift of 5 nm for an ARI variation of 0.003, showing an ARI sensitivity of 1666.67 nm/RIU.

To demonstrate the applicability of our temperature-insensitive bio-sensor and to improve upon the LPFG-based *Escherichia coli* (*E. coli*) bacteria sensor [10], we used it for the quantitative detection of *E. coli* bacteria in water. The *E. coli* is a facultative anaerobic, gram-negative bacterium, with some of its strains (including the O157:H7), being especially deadly to children and elderly patients. A conventional detection method of bacteria consists of an amplification of the signal to confirm the existence of the target microorganism. The amplification often is in terms of the growth of bacterial cells in different media and conditions. Although the amplification-based methods, in principle, are able to detect bacteria, even at a single cell level, the detection process is time-consuming (possibly taking days) to let the bacteria form its colonies. Moreover, the identification of the unknown bacterium takes longer, and a more complex series of tests are needed. Besides the traditional clinical techniques, there are some microbial and molecular techniques that are available today to test the samples [15]. For example, the polymerase chain reaction is a sensitive method that can determine small quantities of genetic material to detect the bacteria [16]. In addition, an immunological method such as enzyme-linked immunosorbent assay (ELISA) is also a specific and sensitive technique [17]. However, both of these cases are time-consuming and require highly qualified personnel, as well as expensive laboratory instruments. To address these challenges, a fast technique that can detect the targeted bacteria in trace amounts and, at the same time, is easy to operate, is highly preferable. For this technique, we first thoroughly cleansed the cladding surface to remove any traces of glycerin, first with distilled water and then with methanol. To use sensor as an affinity sensor, the cladding surface of the sensor was salinized by incubating a number of sensors in APTES ((3-Aminopropyl)triethoxysilane) H2N-(CH2)3-Si-(OCH3)3) diluted to 5% in methanol for about 3 h at room temperature. Reacting with the OH- and $SiO_2$ cladding, the APTES forms an aminopropyl derivative of glass, which is then used as a positively charged adsorbent for affinity sensing. The resulting thin film of amino functional groups exposed on the top of the cladding region was then functionalized by an amine-reactive homobifunctional cross-linker glutaraldehyde (5% in deionized water) for 30 min. After washing the LPFGs again with deionized water to remove the excess glutaraldehyde, they were incubated in T4 bacteriophages ($10^{10}$ pfu/ml [pfu: plaque forming units] for 4 h) to covalently immobilize them on a sensor surface through their amine groups reacting with the biofilm prepared on the sensor surface. Finally, the sensors were washed thoroughly with the PBS buffer to rinse off the excess (unbound) phages, and various concentrations of *E. coli* bacteria were then introduced to the sensor by dipping it into *E. coli* infected water for ~20 min.

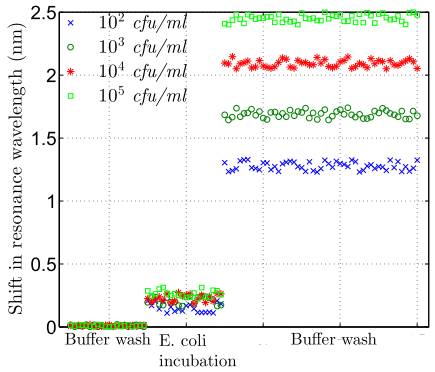


**Fig. 5.** Spectral shift of the sensor at different stages of *E. coli* binding events.

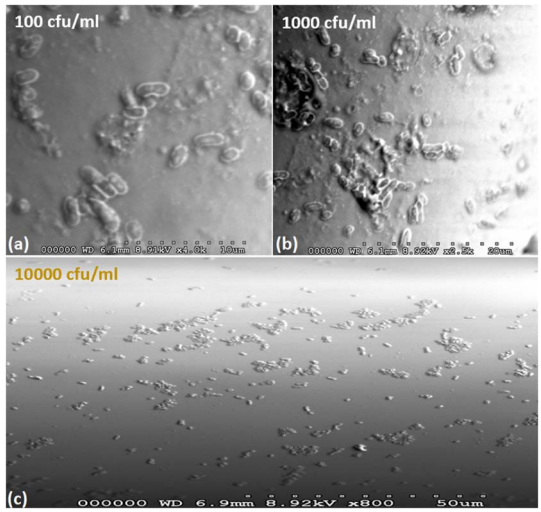


**Fig. 6.** SEM micrographs showing a bacterial binding on the sensor surface at a bacterial concentration of (a) $10^2$ cfu/ml, (b) $10^3$ cfu/ml, and (c) $10^5$ cfu/ml.

The sensor's response during PBS buffer incubation, bacterial solution incubation, and post-*E. coli* PBS buffer incubation is shown in Fig. 5, where distinct spectral shifts for different concentrations of *E. coli* bacteria are demonstrated. To study the effect of the temperature on the sensor, we heated the solution between room temperature (24°C) and 40°C, while continuously recording the resonance wavelength, and the same has been plotted in Fig. 5 which shows a maximum wavelength shift of ∼2.4 nm for an *E. coli* concentration of $10^5$ cfu/ml. A spectral shift of ∼1.3 nm is observed for an *E. coli* concentration of 100 cfu/ml. Assuming a temperature sensitivity of 0.1 nm/°C, for long-period gratings written in SMF-28 fiber [4], the expected temperature-induced spectral shift should be 1.6 nm over the temperature range of our experiments. However, a mere shift of 0.1 nm was observed in our experiments over the entire temperature range (Fig. 5). The small fluctuations in the resonance wavelength can be attributed to the high noise of the optical source at high wavelengths. Finally, to show that the observed spectral shifts are not merely due to the changes in the refractive indices of *E. coli* solutions and that the sensor, indeed, works as an affinity sensor, we recorded SEM micrographs of the sensor surface after incubating it into various concentrations of *E. coli* bacteria. This is shown in Figs. 6(a)–6(c) for *E. coli* concentrations of $10^2$ – $10^5$ cfu/ml. This figure shows that the fractional coverage of the *E. coli* film on the sensor surface increases with the increasing concentration of *E. coli* bacteria in water, resulting in higher spectral shifts of the sensor with an increasing bacterial concentration in water. Our sensor can thus be very efficiently used to detect *E. coli* concentration in water over a wide temperature fluctuation of 24°C–40°C.

In conclusion, in this Letter, we have proposed and demonstrated a very compact and cost-effective bio-sensor with inherent temperature insensitivity. As an example of the bio-sensing capability of out sensor, we carried out experiments to detect various concentrations of *E. coli* bacteria in water kept at different temperatures. We observed a slight fluctuation of ∼0.1 nm in the resonance wavelength, which can be attributed to the noise associated with the source at higher wavelengths. Spectral shifts ranging between 1.3 and 2.5 nm were observed with changing bacterial concentrations. The principle used to obtain the temperature insensitivity can be used in designing various temperature-insensitive fiber-optic devices based on long-period gratings.

**Funding.** Natural Sciences and Engineering Research Council of Canada (NSERC); Industrial Research Chair Program of Canada; Department of Science and Technology (DST), Ministry of Science and Technology INSPIRE (IFA13-PH-69).

## REFERENCES

1. Z. Wang, J. R. Heflin, K. V. Cott, R. H. Stolen, S. Ramachandran, and S. Ghalmi, Sens. Actuators B **139**, 618 (2009).
2. M. J. Yin, B. Huang, S. Gao, A. P. Zhang, and X. Ye, Biomed. Opt. Express **7**, 2067 (2016).
3. D. Sun, T. Guo, Y. Ran, Y. Huang, and B.-O. Guan, Biosens. Bioelectron. **61**, 541 (2014).
4. R. Garg, S. M. Tripathi, K. Thyagarajan, and W. J. Bock, Sens. Actuators B **176**, 1121 (2013).
5. X. W. Shu, B. A. L. Gwandu, Y. Lin, L. Zhang, and I. Bennion, Opt. Lett. **26**, 774 (2001).
6. B. A. L. Gwandu, X. Shu, T. P. Allsop, W. Zhang, and I. Bennion, Electron. Lett. **38**, 695 (2002).
7. Q. Liu, K. S. Chiang, and K. P. Lor, Opt. Lett. **31**, 2716 (2006).
8. H.-J. Chen, L. Wang, and W. F. Liu, Appl. Opt. **47**, 556 (2008).
9. S. M. Tripathi, W. J. Bock, A. Kumar, and P. Mikulic, Opt. Lett. **38**, 1666 (2013).
10. S. M. Tripathi, W. J. Bock, P. Mikulic, R. Chinnappan, A. Ng, M. Tolba, and M. Zourob, Biosens. Bioelectron. **35**, 308 (2012).
11. A. K. Ghatak and K. Thyagarajan, *Introduction to Fiber Optics* (Cambridge University, 1998).
12. K. Okamoto, *Fundamentals of Optical Waveguides*, 2nd ed. (Elsevier, 2006).
13. M. J. Adams, *An Introduction to Optical Waveguides* (Wiley, 1981).
14. R. Kashyap, *Fiber Bragg Gratings* (Academic, 2010).
15. R. Lopez-Roldan, P. Tusell, S. Courtois, and J. L. Cortina, Trend Anal. Chem. **44**, 46 (2013).
16. D. M. Silva and L. Domingues, Ecotox. Environ. Saf. **113**, 400 (2015).
17. I.-H. Cho and J. Irudayaraj, Int. J. Food Microbiol. **164**, 70 (2013).